APL Materials

DNA origami nanorulers and emerging reference structures

Cite as: APL Mater. **8**, 110902 (2020); https://doi.org/10.1063/5.0022885
Submitted: 29 July 2020 . Accepted: 16 September 2020 . Published Online: 10 November 2020

Michael Scheckenbach, Julian Bauer, Jonas Zähringer, Florian Selbach, and Philip Tinnefeld

DNA origami nanorulers and emerging reference structures

Cite as: APL Mater. 8, 110902 (2020); doi: 10.1063/5.0022885
Submitted: 29 July 2020 • Accepted: 16 September 2020 •
Published Online: 10 November 2020

Michael Scheckenbach,[1] Julian Bauer,[1] Jonas Zähringer,[1] Florian Selbach,[1,2,a)] and Philip Tinnefeld[1,a)]

AFFILIATIONS

[1]Department of Chemistry and Center for NanoScience (CeNS), Ludwig-Maximilians-Universität München, Butenandtstr. 5-13, 81377 München, Germany
[2]GATTAquant GmbH, Lochhamer Schlag 11, 82166 Gräfelfing, Germany

[a)]**Authors to whom correspondence should be addressed:** selbach@gattaquant.com and philip.tinnefeld@lmu.de

ABSTRACT

The DNA origami technique itself is considered a milestone of DNA nanotechnology and DNA origami nanorulers represent the first widespread application of this technique. DNA origami nanorulers are used to demonstrate the capabilities of techniques and are valuable training samples. They have meanwhile been developed for a multitude of microscopy methods including optical microscopy, atomic force microscopy, and electron microscopy, and their unique properties are further exploited to develop point-light sources, brightness references, nanophotonic test structures, and alignment tools for correlative microscopy. In this perspective, we provide an overview of the basics of DNA origami nanorulers and their increasing applications in fields of optical and especially super-resolution fluorescence microscopy. In addition, emerging applications of reference structures based on DNA origami are discussed together with recent developments.

I. INTRODUCTION

Light microscopy techniques are major nondestructive imaging tools in biology, biomedicine, and related life sciences. The diffraction limit, the ultimate resolution limitation in optical microscopy, has been overcome with super-resolution (SR) microscopy.[1–3] Even distances below the diffraction limit of light can now be resolved with a non-invasive optical microscope yielding crisp images. The most prominent super-resolution techniques are stimulated emission depletion[4] (STED) and single-molecule localization-based microscopy (STORM,[5] dSTORM,[6] PALM,[7] PAINT,[8] DNA-PAINT,[9] MINFLUX[10,11]) and derivates thereof. Similarly, structured illumination microscopy[12,13] (SIM) techniques are pushing the limits of resolution. The resolution problem boils down to the ability of distinguishing two point-like objects. Two fluorescent spots in close proximity, for example, could not be differentiated in a wide-field microscope [Fig. 1(a)] as quantitatively described by the Rayleigh criterion. The information of the localization of each spot can, however, be reconstructed when just one fluorophore is visible at a time. In single-molecule localization approaches, the point spread function (PSF) of each emitting spot is fitted by a Gaussian function and the exact position is determined with a precision substantially better than the detector pixel size.

In the early years of super-resolution microscopy, filamentous structures such as microtubules and actin filaments were imaged to demonstrate the new techniques and their variants [Fig. 1(b)].[14] The images were then examined to find the smallest features that could be distinguished. This could, e.g., be two filaments oriented parallel over some distance. Presenting cross sections of these parts of the image demonstrated the achievable resolution. The disadvantages of this approach are obvious. First, the true underlying structure is unknown. The measurements are not reproducible as every location in a cell is different and statistically underpinned resolution measures cannot be deduced. Critically, claimed resolution measures cannot directly be reproduced in another laboratory. The important property of a standard, i.e., providing comparability between labs and instruments was not provided. Furthermore, the molecular environment of the labels is not defined and the number of labels contributing to the signal is not known.

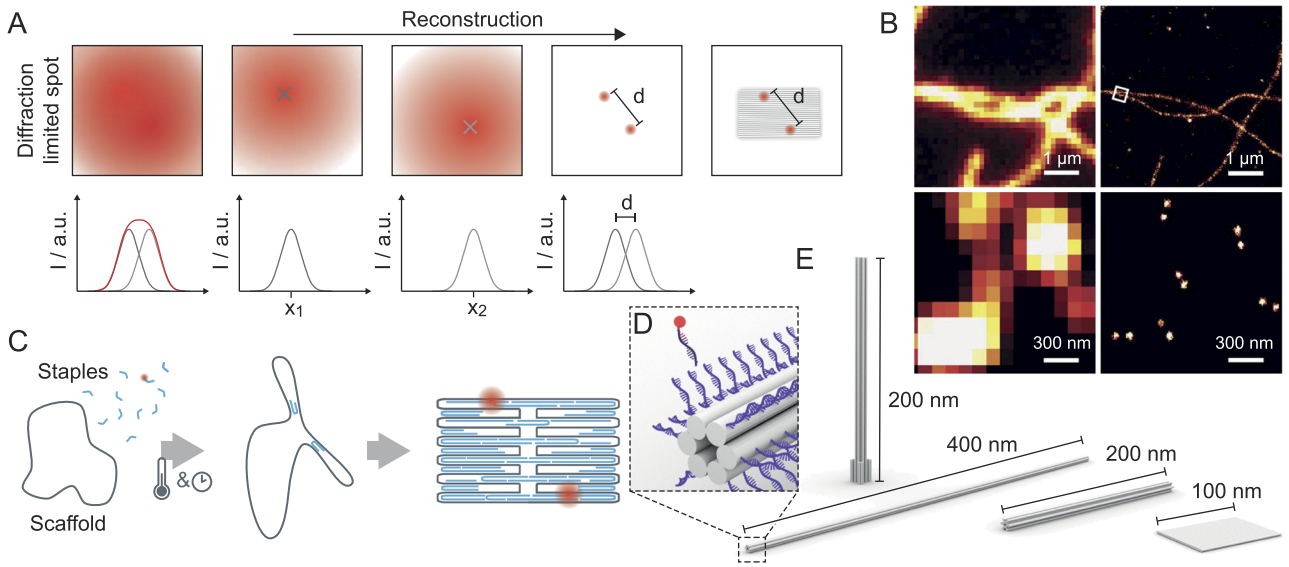

FIG. 1. (a) Sketch explaining super-resolution microscopy by successive single-molecule localizations. Positions of individual, independently switching molecules are determined and the super-resolution image is reconstructed from the density of localizations. (b) Comparison of actin filaments (top row) and DNA origamis (bottom row) as test structures. Right panels show representative super-resolution images and left panels show the corresponding total internal reflection fluorescence (TIRF) images (adapted from Ref. 14). (c) Scheme of folding a dye labeled DNA origami nanoruler. (d) Scheme of addressability of modifications (e.g., fluorophores) on DNA origami nanorulers by DNA hybridization. (e) Scheme of underlying structures successfully used as DNA origami nanoruler breadboards [six helix bundle (400 nm), 12 helix-bundle (200 nm), rectangular structure (100 nm), and pillar (200 nm)].

Nowadays, three approaches have evolved for objective characterization of fluorescence imaging techniques including algorithmic resolution calculation[15] [e.g., Fourier ring correlation (FRC)[16]], defined natural protein structures such as nuclear pores[17,18] or the diameter of microtubules,[18] and artificial structures such as DNA origami nanorulers.[19–23] Among the different approaches which all have their pros and cons, DNA origami nanorulers are the best-defined and most versatile and realistically allow emulating diverse microscopy experiments. As is shown in Fig. 1(b) (bottom panel), the ability to distinguish two point-light sources as required by established resolution criteria is directly visualized for the imaging technique in the bottom right panel compared to the imaging method used for the image in the bottom left panel. Beyond the possibility to quantitatively characterize microscopy techniques, DNA origami nanorulers have become a positive control, calibration tool, and training sample in fluorescence microscopy and beyond.

In this perspective, we outline the development of DNA origami nanorulers, explain the principles of their design and functioning, and provide numerous examples of their application. These applications meanwhile diverge into different fields and an outlook on new directions is given. Emerging applications include fiducial markers (FM), brightness referencing and applications in atomic force microscopy, electron microscopy and their combinations.

A. DNA origami nanorulers - basics

DNA origami nanorulers[14] are building on the DNA origami technique. DNA origami was introduced in 2006 by Rothemund and is seen as a milestone in DNA nanotechnology.[24] With DNA origami, a single person can easily create impressively big DNA nanostructures with programmed geometry and almost atomistic structural control.[24,25] The resulting nanostructures are obtained in high yields and, after folding, they are robust and stable in a variety of conditions and over long timescales. DNA origami nanorulers made early use of DNA origami and led to the first commercial application based on DNA origami technology by the spin-off company GATTAquant.

DNA origami are built from one long single-stranded DNA of ~7300 nucleotides with known sequence, which is called the scaffold strand. The single-stranded, circular scaffold strand was obtained from a bacteriophage (typically M13mp18) and can be folded with ~200 shorter oligonucleotides, so called staple strands into a defined 2D- or 3D-structure [Fig. 1(c)].[25] Scaffold and staple strands are mixed together, heated, and cooled down slowly to room temperature to ensure correct DNA hybridization of the individual parts. DNA origami structures can be designed with open-sourced software like caDNAno[25] or canDo.[26] First, with the aid of caDNAno, the user decides on the geometry of the structure and the scaffold is routed through this geometry to obtain the desired shape. Subsequently, the staple strands are planned so that parallel DNA helices are connected by crossovers and the final structure is stabilized. The conformational flexibility of the planned structure is estimated with the software canDo. At the end of the design process, a list of staple strands to be purchased for synthesis is obtained. To get from DNA origamis to DNA origami nanorulers, certain staples strands are modified, e.g., with fluorescent dyes. As each staple position in the DNA origami is precisely known, the exact position of the fluorescent dyes in the DNA origami is well-defined.[27]

Alternative to fluorescent dyes, a multitude of chemical functionalities including amino- or thiol groups, biotin, cholesterol, pyrene, and click chemistry groups can thus be introduced in pre-defined patterns at well-controlled stoichiometry providing the chemical handles for placing proteins, nanoparticles, and essentially everything that is compatible with the water chemistry of DNA. Another simple and versatile attachment chemistry can be offered by extending the staple strands so that single-stranded DNA oligonucleotides protrude from the DNA origami to which other DNA functionalized moieties can bind.[28] Protruding single-stranded DNA is also used for the super-resolution technique DNA-PAINT that is the basis of one of the most important realizations of DNA origami nanorulers.[9,20,29]

For designing a DNA origami nanoruler, simple geometric considerations are made. Along the direction of the DNA helix, the distance between two adjacent bases is 0.34 nm and the distance between the centers of two neighboring DNA helices is between 2.5 nm and 2.8 nm depending on the exact origami design (e.g., honeycomb or square lattice) and the buffer conditions.[30,31] Still, the finally measured distance in a DNA origami nanoruler rarely exactly meets the designed distance as over larger distances further aspects such as strain, torsion, and bending come into play.[14,19,32] Additional distance inaccuracy comes from incorporation efficiency of modified staple strands, docking site accessibility of external modifications, and length and flexibility of used dye linkers to the DNA.[33] Hence, accurate distances have to be determined by microscopes that are able to resolve the structure and are calibrated to determine the distances.[19,28] With this procedure, accurate placement (<1 nm) can be achieved.[28,32,34]

Fundamentally, fluorescent dyes can be incorporated at every base position of the DNA origami. At very small distance (<5 base pair distance), however, quenching occurs as soon as the dyes physically touch.[35] For larger distances, fluorescence scales perfectly linear with the number of dyes.[19,20] In practice, fluorescent dyes are commonly incorporated by labeling staple strands at the 3′- or 5′-end, which is also more economical. To this end, the number of fluorescent dyes per DNA origami is limited to roughly 1000 for a maximally labeled DNA origami still avoiding quenching and to about 200 dyes for singly labeled staple strands. For a 12 helix-bundle (12 HB), i.e., a typical DNA origami nanoruler structure that has a length of roughly 200 nm and a diameter of ~13 nm, this means that we find one potential dye position every nanometer along its 1D projection [see Fig. 1(d)]. In simple terms, the 12 HB is a DNA origami nanoruler that can be seen as a molecular breadboard with one plug-in position every nanometer.

Besides the 12 HB, typical DNA origami structures used for DNA origami nanorulers are rectangles and rod-like structures such as DNA bundles (e.g., 6 HB) [see Figs. 1(d) and 1(e)]. The rectangular structure enables modifications over the whole 2D breadboard structure and the 6 HB is so long that a nanoruler with marks at its ends can be resolved with conventional fluorescence microscopy.[20] For 3D applications, a pillar-like structure was designed that can specifically be immobilized via its small base using biotin modifications on streptavidin surfaces and stands roughly 200 nm high despite its enormous aspect ratio.[23,36]

In the following, we describe more specific applications of DNA origami nanorulers. We chapter the methods into the more general stochastic switching (also referred to as single-molecule localization methods) and targeted switching super-resolution approaches[37] and report on the strength of these tools in atomic-force microscopy (AFM) and transmission electron microscopy (TEM). Finally, we outline emerging DNA origami applications in which they are used as reference structures.

II. STOCHASTIC SWITCHING BASED SUPER-RESOLUTION MICROSCOPY NANORULERS

The principle of the reconstruction of stochastic single molecule localizations shown in Fig. 1(a) can be accomplished by different approaches as, for example, covered in the following reviews.[1,38,39] Most common single-molecule localization techniques use either the stochastic activation of photoswitchable fluorescent molecules such as fluorescent proteins and certain organic dyes (STORM,[5] PALM,[7] GSDIM,[40] SOFI[41]), or the stochastic binding of fluorescently labeled molecules to a target (PAINT,[8] uPAINT,[42] DNA-PAINT[9]).

All of these SR methods work with image reconstruction, implying that the true image cannot be immediately deduced from the acquired data, but lies beneath layers of data processing, like localizing, un-drifting, and other corrections. Single-molecule localization super-resolution methods especially require optimization of the measurement parameters and the sample preparation. For sample preparation, dense enough labeling and a high enough number of localizations have to fulfill resolution requirements of the Nyquist criterion.[43] Due to the number of factors and the indirect and algorithmic procedure to obtain the final image, resolution is not solely defined by localization precision. It is therefore vital to verify the performance of the setup and to test whether a claimed resolution can indeed be achieved. Further, to ensure only one emitting molecule at a time within a diffraction limited region, the blinking kinetics have to be adapted accordingly. Here, a positive control is helpful for adjusting the photoswitching, blinking or dye binding kinetics to the measurement method that depends amongst others on buffer compositions and laser excitation conditions. The latter requires that the positive control uses the same fluorescent dyes in a similar environment. All these arguments call for reliable and well-defined structures in the nanometer regime that can be adapted to the needs of the specific method and even for the fluorescent dye used. Here, the introduced DNA origami nanorulers serve as an established reference tool, offering a quantitative analysis of the resolution, e.g., a multi-Gaussian fit to the line profile along a 12-helix bundle DNA origami with three equidistant spots is a measure of the optical resolution [Fig. 2(a)].[28] To answer the question of the accuracy of nanorulers, a strategy was developed to quantify the traceability of DNA origami nanorulers in SI units, establishing them as true standards. Accordingly, the accuracy, and not only the precision of the nanorulers, was characterized and found that the accuracy of marks (labeling spots) on DNA origami was commonly better than 2 nm.[28] Many labs meanwhile use DNA origami nanorulers to first check and demonstrate their SR abilities and then present their biological results obtained by SR microscopy.[44–49]

Besides, for the investigation of a new method for the spectral filtering of fluorescent impurities,[50] DNA origami nanorulers are often used to demonstrate the ability of new software and hardware tools. Parameter free resolution estimation in single images[15,51] and data processing methods for cluster analysis[52–54] utilize DNA

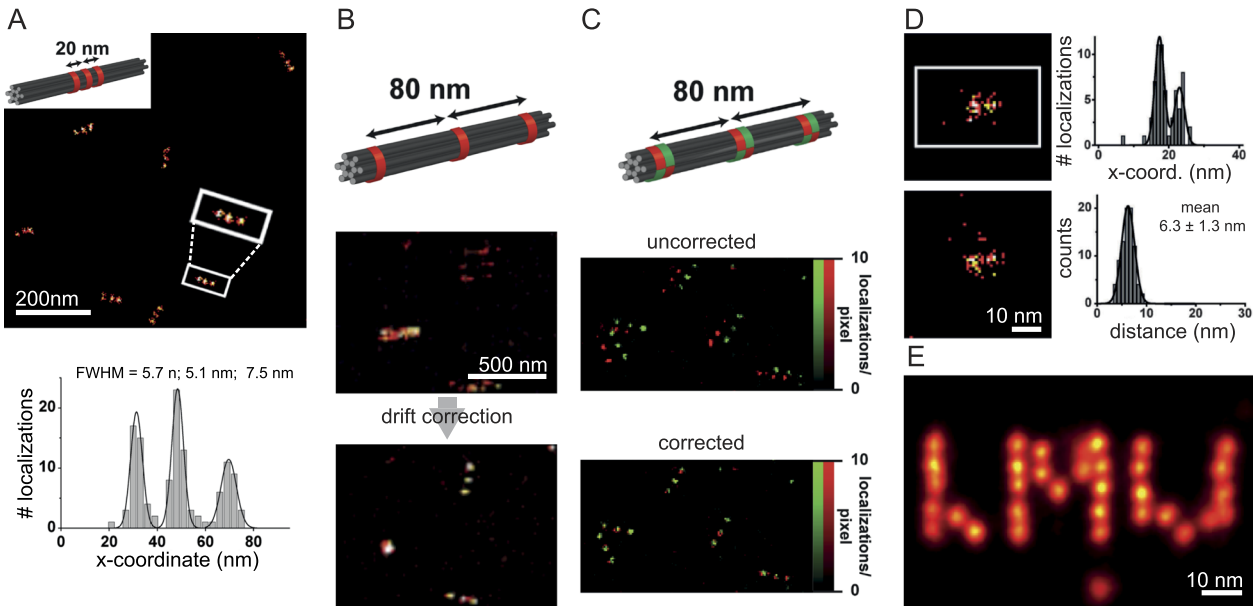

FIG. 2. Super-resolution microscopy with DNA-PAINT. (a) Nanorulers with 20 nm spacing between marks. The histogram shows the accumulated profile of a representative nanoruler (white frame) and is fitted with a triple gaussian.[28] (b) Fiducial marker (FM) and nanorulers with 80 nm spacing imaged simultaneously (upper image). Below, the same image, drift corrected using the positions of the FM.[62] (c) Two-color overlaid super-resolution images of nanorulers with 80 nm spacing between dual-color labeled marks before and after correction of the chromatic shift. The chromatic correction was calculated in a separate measurement of dual-color labeled DNA origami FMs.[28] (d) Single DNA origami structures with docking sites at a designed distance of ~6 nm. The upper histogram shows the accumulated profile of one representative DNA origami (white frame), fitted with a double Gaussian. The bottom histogram shows the distribution of many measured distances fitted with a Gaussian.[21] (e) Average image of 215 DNA origami structures with the letters "LMU." The distance between adjacent spots are ~5 nm.[60]

origami nanorulers as verification tool for their performance. Hardware improvements of microscopy setup components are also demonstrated with nanorulers as reference tool. This includes the introduction of a chip-based waveguide, which decouples the total internal reflection fluorescence (TIRF) illumination from the detection path,[55] the development of SPAD arrays for widefield applications,[56–58] and active stabilization of the sample throughout the measurement to reduce its drift.[59]

Sample drift is a crucial problem in SR microscopy. Whereas focus drift in the axial direction leads to an irretrievable loss in localization precision, a sample drift in the x–y-plane can be corrected for. Freely available and widely used localization software like Picasso[60] or ThunderSTORM[61] can use cross-correlation or fiducial-based alignment algorithms to back-calculate the x–y drift. For sufficient numbers of localizations, the cross-correlation can undrift the sample structures to a certain extent. A more precise and stable approach tracks the continuous signal from additional fiducial markers (FM) in the sample[62] [Fig. 2(b)]. However, the use of FM implies a reduced sample density to guarantee the diffraction limited separation of the continuous signals.

Besides the sample movement induced shifts, experimenters can also be confronted with steady shifts, e.g., chromatic aberrations induced by the optical elements in the detection path. For these shifts, a correction vector map can be generated by measuring dual color FM, or other structures, where fluorophores of both colors can be localized at the same position. This map can be evaluated in calibration measurements for linear shifts[28] [Fig. 2(c)], or, analogously, for radial and combined shifts.[63]

DNA origami FM used for the corrections above can be realized with fluorophores incorporated in a DNA origami structure making them also subject to photobleaching. More elegantly, DNA origami FM can be incorporated with many identical binding strands for DNA-PAINT. Renewal of labeled strands makes them free of photobleaching, maintaining a steady intensity trace, even throughout long measurements.[60] To reduce the background, one can use the same labeled imaging strands as for the structure under investigation.

In general, DNA-PAINT has recently attracted attention as the required dye blinking is separated from the photo-physics of the dyes so that the full photon budget of the brightest dyes can be used and multiplexing is facilitated using orthogonal binding sequences. Moreover, DNA-PAINT provides an additional information channel from examining the binding kinetics.[64,65] In recent publications, optimization of the binding kinetics was used to decrease the SR imaging time to the order of a minute.[66,67] Historically interesting, DNA-PAINT was first developed on DNA origamis and in conjunction with DNA origami rulers.[9,14] With DNA-PAINT labeled DNA origami structures with a spot distance of 6 nm could be resolved already in 2014 [Fig. 2(d)],[21] which was excelled in 2017 with 5 nm distances resolved in grid arrangements of dyes with ~1 nm precision, representing the letters "LMU" [Fig. 2(e)].[60] The latter study showed that the labeled DNA origami structures can

also be used as FM to undrift the sample. Other commonly used FM are gold nanoparticles (AuNPs), quantum dots, and fluorescent microspheres.

Over the last decade, SMLM advanced into the third dimension. Common methods use either the biplane approach[68] or astigmatism[69] to image in an axial range of several hundred nanometers. The ability of resolving several tenth of nanometers adds additional value to well-defined 3D DNA origami structures. The so-called nanopillars with 80 nm spot distance and arbitrary spatial orientation in the sample were first resolved under the use of astigmatism[23] and served as reference tool for a quantitative analysis on the performance of a 3D SR microscopy setup with the biplane approach[63] [Fig. 3(a)]. The option of attaching nanoparticles to DNA origami structures was used for a study of the shift of fluorescent signals induced by plasmonic nanoparticles placed in proximity of a fluorescent dye [Fig. 3(b)].[70] This can be visualized in 2D [red-yellow color code in left panels of Fig. 3(b), gray overlay indicates scattering of the nanoparticle] and 3D [blue-red color code in right panels of Fig. 3(b)], whereas the 3D imaging is essential for the quantitative estimation of the shift. In addition, flow cytometry recently advanced toward 3D imaging [Fig. 3(c)].[71] The SR of the two spots, labeled with different colors with 180 nm distance, was achieved by dual channel acquisition. A reference measurement with beads mapped the astigmatic change of the PSF to an axial position in the flow chamber (indicated with 1, 2, 3). The designed distance could then be recuperated from the distribution of several hundred nanorulers passing the field of view (FOV) one by one.[71]

Standard and customized DNA origami nanorulers are commonly available for all stochastic SMLM techniques mentioned in this paragraph. For TIRF microscopes, independent of the imaging technique of choice, sealed and "ready to image" DNA-PAINT samples can be purchased. A recent publication might even establish DNA-PAINT for HILO or EPI illumination.[72]

III. TARGETED SWITCHING SUPER-RESOLUTION NANORULERS

The second approach of super-resolution microscopy uses targeted switching of fluorescent molecules by using patterns in the excitation pathway and exploiting saturable transitions.[37] Stimulated emission depletion (STED) nanoscopy is a prominent example for these coordinate targeted techniques and overlays a donut-shaped depletion beam on a Gaussian excitation, hence reducing the effective detection volume.[4,73] The requirements for microscopy with targeted readout are different and therefore also need different DNA origami nanorulers. One major difference is that several dyes are allowed to fluoresce at the same time. Here, the versatility of DNA origami nanorulers can be seen in a wide range from diffraction limited to nanometer precise placements of dyes.

The most broadly used microscopy technique with structured illumination is confocal microscopy. Not being a SR technique, it requires diffraction limited samples, hence dyes separated by 386 nm on a six helix-bundle can be resolved [Fig. 4(a)]. For confocal

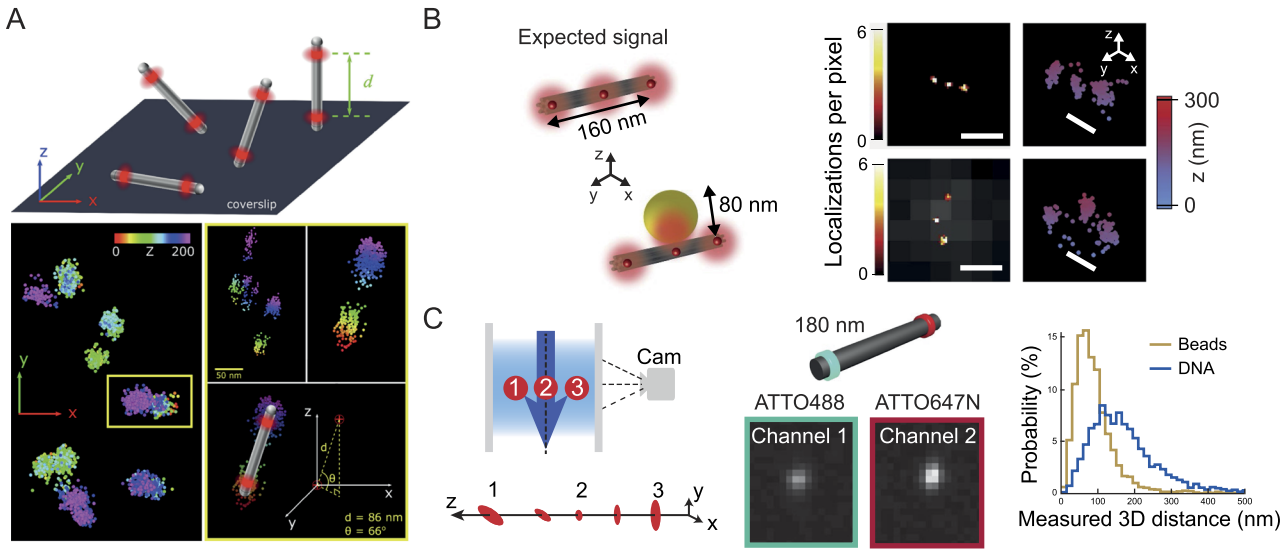

FIG. 3. (a) 3D DNA-PAINT image of 3D nanopillars with 80 nm spacing using the biplane method. The upper sketch shows nanopillars indicating a broad distribution of orientation. On the left is a 2D view of localization clouds in the x–y plane with color encoded z-position. An exemplary nanopillar (yellow frame) is depicted before (left) and after (right) drift correction and analyzed for the spatial separation and the angular orientation of the two spots (bottom).[63] (b) Molecular localization shift by plasmonic coupling. A sketch depicting the expected emission spots with and without the presence of a gold nanoparticle next to the respective 2D DNA-PAINT images (scale bars, 200 nm) and 3D DNA-PAINT images (scale bars, 100 nm).[70] (c) Multicolor 3D localization flow cytometry. A cylindrical lense in the detection pathway resolves the z positions (1, 2, 3) in the flow cell with astigmatism. Nanorulers, labeled with red and green dyes (180 nm distance between marks), are simultaneously detected in two color channels. From the respective x–y position (pinpointed by a gaussian) and the z position (estimated by the ellipticity of the PSF), distances between marks can be calculated in 3D. The histogram shows the measured distances of numerous nanorulers.[71]

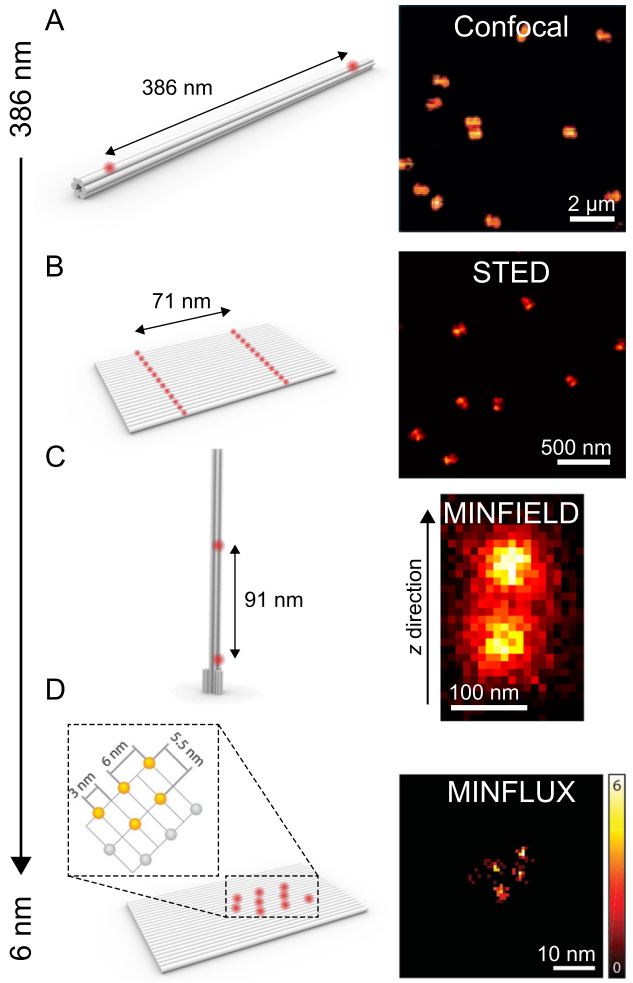

FIG. 4. DNA origami nanorulers across length scales for SR based on targeted switching. (a) Nanoruler for diffraction limited microscopy. On the left, a six helix-bundle labeled with two fluorophores in 386 nm distance is shown. Thus, the DNA origami is resolvable with standard confocal microscopy, which is shown on the right.[20] (b) Nanoruler for 2D STED microscopy: The sketch on the left shows a rectangular DNA origami labeled with two parallel lines of fluorophores at a distance of 71 nm. The panel on the right shows that these lines are resolved with STED microscopy.[20] (c) Nanoruler for 3D MINFIELD-STED microscopy. On the left, an upright 12 helix-bundle is shown and is labeled with single fluorophores at a distance of 91 nm. This 3D structure is resolved using MINFIELD-STED microscopy on the right.[82] (d) Nanoruler for MINFLUX nanoscopy. On the left, the labels on a rectangular DNA origami are indicated. On the right, using MINFLUX nanoscopy, the blinking fluorophores are resolved with 1 nm precision.[10]

microscopy, the applications range from calibration of the setup to training of experimenters.[20]

While the performance of a confocal setup can be calculated via Abbes formulas, this is not as straight-forward for SR setups, like STED microscopes. Here, the resolution is mainly dependent on the power of the depletion beam, however, also sample properties, e.g., the dyes themselves as well as photobleaching have an influence on the resolution.[29] Hence, the effective resolution needs to be accessed experimentally.[74] Thanks to the robustness and homogeneity of DNA origami nanorulers in signal and size, they are routinely used to resolve inter-mark distances down to few tens of nanometers, demonstrating that the SR setup can resolve the structures of interest [Fig. 4(b)]. These samples are mostly of biological nature and gave insights, e.g., in the actin/spectrin organization at synapses using 3-colors multilevel STED,[75] the γ-secretase in neural synapses[76] or topoisomerase in mitochondria.[77]

With increasing STED laser powers and improved resolution, the volume from which fluorescence is still allowed is decreasing so that fewer and fewer molecules are contributing to the signal and the background increases due to the high overall laser power. Resolution can then be limited by the signal-to-noise ratio and common fluorescent beads are either too big or not bright enough for optimal quantification of the STED abilities. To this end, DNA origamis can offer point-light sources with maximized brightness density. A typical DNA origami structure with 23 nm diameter could, e.g., be labeled with ~80 dyes and immobilized for STED imaging. With these DNA origami nanobeads, optimized point-spread-functions for STED deconvolution imaging were obtained that could not be matched with conventional fluorescent beads.[78]

The choice of dyes is another important aspect for optimizing STED microscopy. Using DNA origami nanorulers, different dyes were tested under different conditions.[79] In addition, the multiplexing possibility of DNA-PAINT was exploited in combination with STED by alternating washing and labeling steps of DNA origami structures.[80,81] Importantly, multiplexing was achieved with a single color system by encoding the different labels in the DNA sequences used for labeling.[79]

As DNA origami nanorulers are established, not only resolutions on existing methods are checked but also proof-of-principle measurements of new more powerful techniques are demonstrated with DNA origami nanorulers as the reference structure. One example is the introduction of the STED modality MINFIELD-STED. MINFIELD is an imaging strategy that increases resolution by reducing the exposure and hence the photobleaching.[82] With MINFIELD-STED, 2D objects smaller than 25 nm were resolved, as well as 3D DNA origami nanorulers with an axial precision of 60 nm [Fig. 4(c)]. Furthermore, other advances of STED nanoscopy, e.g., faster STED by parallel sub-second electro-optical-STED,[83] or in extended sample regions[83,84] were first demonstrated with DNA origami structures.[85,86]

The latest step in resolution of optical nanoscopy was the combination of advantages of single-molecule localization microscopy and excitation patterning shown in the so-called minimal photon flux nanoscopy (MINFLUX).[10,11] MINFLUX nanoscopy localizes the dye in the minimum of four donut-shaped beams, reaching localization precision in the single digit nanometer regime with less than 100 photons per localization, as well as enabling the tracking of quickly diffusing molecules. To be precise, MINFLUX requires stochastic switching for superresolution but was classified in this section due to the similarity of laser profiles. Proof-of-principle measurements were performed on DNA origami nanorulers, which resolved several dyes in less than 6 nm distances with a precision of less than 1 nm in 2D as well as 3D.[20] Here, several dyes were placed on a DNA origami nanoruler and activated stochastically and it was demonstrated that better localization precision could be

achieved with fewer detected photons. Similarly, other techniques called SIMFLUX[87] or Rose[88] use the idea to combine a structured illumination and its emission information to enhance the resolution twofold. Again, proof-of-principle measurements were shown with DNA origami nanorulers.

IV. ENERGY TRANSFER NANORULERS

The breadboard character of DNA origami nanorulers makes them an ideal tool to investigate distance dependent energy transfer mechanisms at the single-molecule level. Förster resonance energy transfer (FRET) ensemble studies using donor–acceptor labeled poly-proline were first conducted in 1967, showing higher FRET efficiencies than expected.[89] To investigate this discrepancy, rigid DNA origami blocks have been used as reference structures for quantitative single-molecule FRET studies. Placing donor and acceptor dyes on the surface of a DNA origami block with known distances reduces the influence of the dye linkers and circumvents the need for a multiparametric fit in comparison to commonly used dsDNA constructs.[90] Furthermore, FRET was used in combination with DNA origami nanostructures in 2009 to probe the controlled opening and closing of the dynamic lid of a DNA origami box designed for applications such as drug delivery [Fig. 5(a)].[91] Besides energy transfer between organic dyes, interactions of dyes with different materials ranging from nanoparticles to metallic surfaces are possible to be investigated in a highly controlled manner using DNA origami nanostructures. Analogously to FRET studies, nanoparticle or metallic surface induced quenching effects were examined with respect to fluorescence intensity, as well as fluorescence lifetime.[92] DNA origamis were used to position AuNPs at varying distance to a dye, and the quenching effect and its distance dependence were elucidated. Additionally, the precise positioning of AuNPs in close vicinity to a fluorophore can be used as a plasmonic nanoantenna. Placing a single fluorophore in the plasmonic hotspot induced by a single or multiple AuNPs, the fluorescence brightness is enhanced up to more than 400 fold.[93,94] Even further, a combination of AuNPs and FRET was already investigated and depending on the conditions, an enhancement of FRET rates could be found [Fig. 5(b)].[95,96] In addition, the coupling of plasmons on the DNA origamis itself as nanowires was demonstrated.[97]

A dye in an excited state can transfer its energy not only to metallic nanoparticles, but also to a metallic surface. The immobilization of 3D DNA origami structures with labeled fluorophores on such metallic surfaces enables the investigation of the z dimension due to the height dependent energy transfer [Fig. 5(c)]. This approach was used to study quenching effects of fluorophore labeled nanorulers to a gold surface, which later could be used as a calibration structure to deduce the height information of the labeled fluorophores.[98] Recent advances with the combination of semi-metallic graphene were made to increase the z-resolution to nanometer precision [Fig. 5(d)], which can be combined with SR microscopy techniques like, e.g., DNA-PAINT or MINFLUX to realize highly sensitive 3D SR microscopy.[99,100]

V. BRIGHTNESS REFERENCING AND EMERGING APPLICATIONS

A. Expansion Microscopy

Another approach to SR is physical expansion of the sample so that initially unresolvable distances are increased to values larger than the diffraction limit to achieve SR information. One advantage is that SR is achieved with common diffraction limited microscopy techniques. In expansion microscopy (ExM), the sample is embedded in an electrolytic polymer [Fig. 6(a)] to which the fluorescent labels are crosslinked.[101] After degradation of the sample, the polymer gel is expanded by dialysis with water. With conventional ExM,

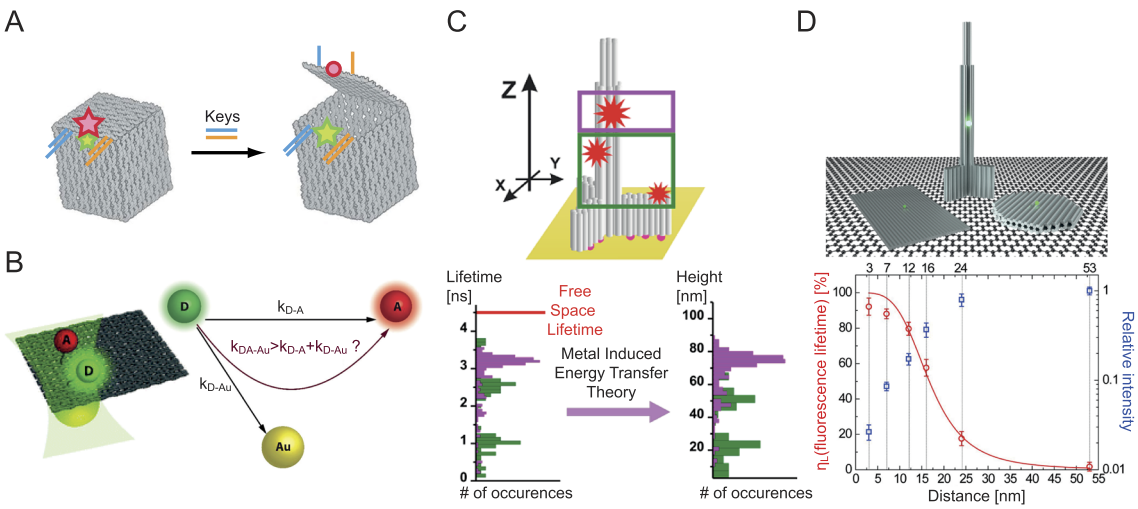

FIG. 5. (a) A box shaped DNA origami with a green and a red dye as a FRET pair, which acts as an opening sensor.[91] (b) Positioning of a donor dye, an acceptor dye, and a gold nanoparticle for the investigation of energy transfer rates. It was shown that an AuNP can enhance the FRET rate.[95] (c) Gold surfaces or semi-metallic surfaces like graphene act as powerful quenchers, which can enable nanometer resolution along the optical axis.[98–100] (d) Positioning of dyes on graphene with DNA origami nanopositioner yields quenching of intensity and fluorescence lifetime of a dye depending on its height with a d^{-4} distance dependence.[99]

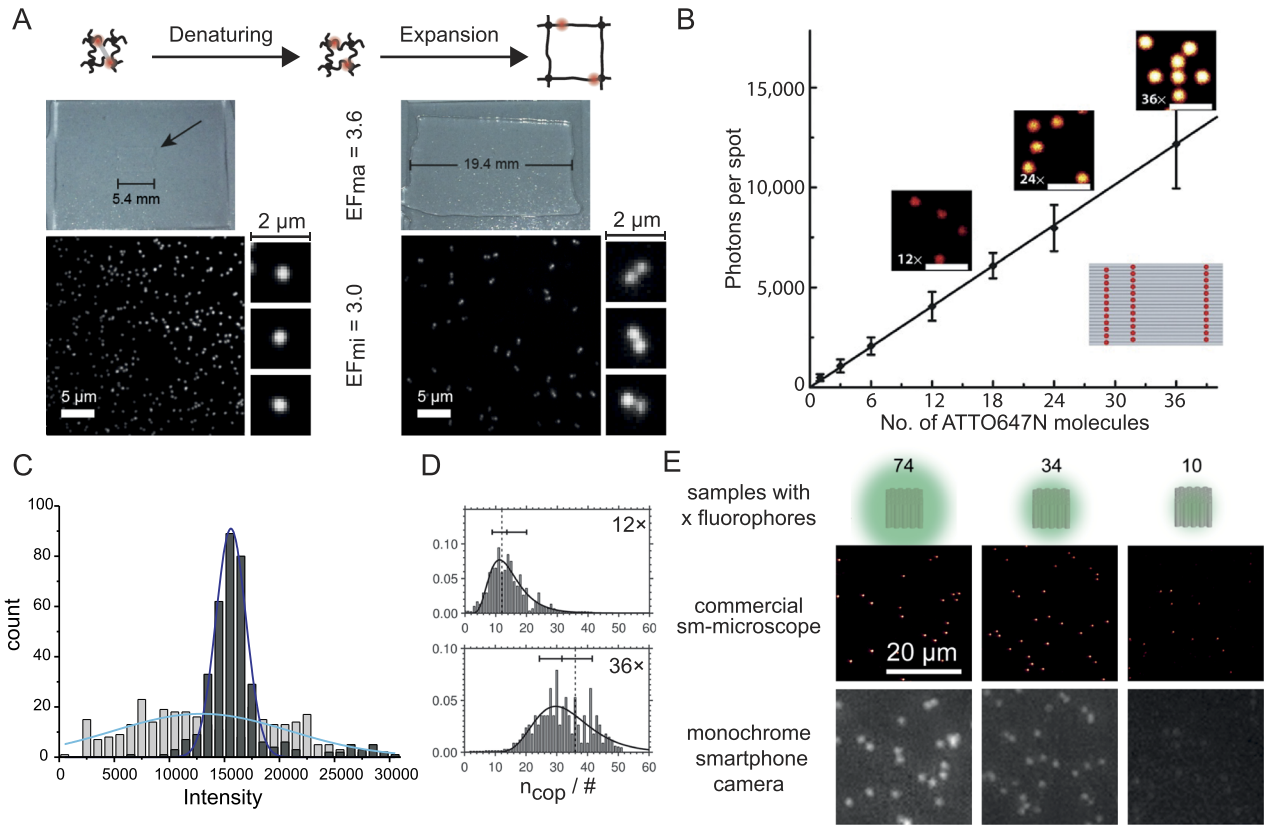

FIG. 6. (a) Top: Polyacrylamide gel before (5.4 mm average width) and after expansion (19.4 mm average width) with a macroscopic expansion factor of 3.6. Bottom: TIRF microscopy image of immobilized nanorulers before gelation and expansion carrying ATTO647N dyes. After expansion nanorulers are imaged in epi-fluorescence and the 160 nm intermark distances are clearly resolved, represented by two adjacent spots (selected zoom-ins).[105] (b) Rectangular DNA origami as fluorescence brightness standard. Top insets, fluorescence images of 12×, 24×, or 36× ATTO647N dyes on the DNA origami. Bottom inset is the sketch of nanoruler with 36× dyes. Scale bars, 2 μm; color scale from 15 to 100 counts.[20] (c) Counting dyes by means of photon statistics. Probability density of estimated emitter numbers from rectangular DNA origami with 12× and 36× ATTO 647N dyes. A log-normal fit to the probability density is depicted as a solid line. Box plot indicates the central 68% quantile about the median of the probability density. The dashed line represents the expected emitter number.[79] (d) Brightness distributions of DNA origami nanobeads (GATTA-Beads, 23 nm) and conventional polystyrene beads (FluoSpheres, 40 nm) reveal the superior homogeneity of DNA origami based nanobeads.[79] (e) Images of highly labeled DNA origami nanobeads (10×, 34×, and 74× dyes) taken with a commercial super-resolution microscope and a monochrome smartphone camera-based fluorescence microscope. The scale bar is applicable to all images.[107]

macroscopic expansion factors of 3–5× are usually achieved, while further increased resolution factors are realized with more sophisticated techniques like iterative ExM (up to 20fold) or by a combination of ExM with SIM.[102–104] Generally, the expansion factor is determined at the macroscopic scale, i.e., by examining the macroscopic swelling of the gel. However, several parameters are critical for characterizing ExM including the expansion factor, cross-linking efficiency, the fraction of active dyes after expansion, and so on. Using nanorulers with inter-mark distances of 160 nm, it could be shown that nanorulers could efficiently be expanded yielding bright marks that could be resolved with conventional microscopy [Fig. 6(a)].[105] Interestingly, the microscopic expansion factor yielded smaller microscopic expansion factors of 3.0 compared to a macroscopic expansion factor of 3.6, which could be explained by the surface immobilization of the DNA origami nanorulers. For a quantitative interpretation of biological expansion microscopy, nanorulers as *in situ* references could also be helpful to reveal anisotropy in the expansion process.

As SR techniques, especially MINFLUX, probe the single nanometer regime, a particular interest of DNA origami nanoruler is how close two dyes can be placed. On one hand, the placement of dyes is DNA-base pair specific, and on the other hand, dye–dye interactions may occur. Hence, DNA origami nanorulers were used as a breadboard to investigate the intensity and lifetime of two dyes in a single base pair precise distance.[35] It was found that, in the case of ATTO 647N at small distances, the lifetimes and intensities of the dyes decrease, which is due to the static quenching of H-type dimer formation. Hence, two independent dyes on a DNA origami nanoruler are limited to a minimal distance of seven base pairs, which equals ~2.3 nm. This leads to the conclusion that in total more than 1000 dyes can be placed on a single DNA origami structure without losing the intensity signal. Together with the highly

controllable breadboard character of DNA origami nanorulers, this naturally leads to DNA origami structures as brightness standards. This is especially interesting for the characterization of the PSF for donut-shaped beams, commonly used in STED and MINFLUX.[11]

B. Brightness referencing

The quantification of labeled dye numbers, i.e., counting the individual fluorophoric labels, plays a key role in the investigation of biological processes as, e.g., in the determination of protein rates and protein complex stoichiometries or the deduction of mathematical models.[106] As discussed in the introduction, appropriately labeled DNA origami structures show a linear dependence of signal intensity on the number of incorporated dyes [Fig. 6(b)].[19,20,107] Together with the stoichiometric control of incorporation, DNA origami nanostructures can thus be used as quantitative signal references. Using DNA origami brightness references, a sensitivity scale of units of fluorescent molecules could be introduced similar to the MESF (molecules of equivalent soluble fluorochrome) that is used in cytometry. In this context, the advantage of DNA origami reference samples (also called DNA origami beads) is that the same dyes as for the sample of interest can be used and the dyes are in a similar chemical buffer environment to the sample in contrast to plastic beads commonly used in flow cytometry.[108] Additionally, recent applications of spectroscopic barcoding in cytometry, i.e., the multicolor and multi-stoichiometric labeling of molecules of interest, require the exact determination of the number of labeled dye molecules with single fluorophore sensitivity.[109]

Counting molecules is also important in microscopy to determine how many labeled molecules contribute to a signal. Counting molecules by intensities has the disadvantage that intensity is an extensive variable. For developing alternative techniques, the photon statistics has for example been used also using DNA origami nanorulers. Techniques like "counting by photon statistics" (CoPS)[110] use the idea of photon antibunching to deduce the number of independent emitters and their molecular brightness [Fig. 6(c)].[85] Here, DNA origami nanorulers with their controllable number of dyes were used as proof-of-principle samples, resolving the number of physical emitters.

The potentially large labeling density of DNA origami nanorulers and the high control over the labeling stoichiometry enable the design of compact and very bright fluorescent beads. Commercially available DNA origami based fluorescent beads show an improved homogeneity and flexibility compared to other conventional beads [Fig. 6(d)]. Such DNA origami nanobeads could be used, e.g., in the determination of PSF in 3D STED microscopy.[79] Highly labeled DNA origami brightness references have also been applied for probing the sensitivity of other types of microscopes. In the recent past, smartphone-based fluorescence microscopy (SBFM) has, for example, evolved as a promising approach to various applications in point-of-care (POC) diagnostics like quantification of immunoassays, detection of microorganisms, or sensing of viruses.[107,111] Although SBFM creates a promising low-cost and field-portable solution, high detection sensitivity comparable to laboratory-based fluorescence microscopes is necessary for the detection of target substances at the single-molecule level. DNA origami nanobeads with up to 74 labeled fluorophores were used to quantify the detection sensitivity of a SBFM [Fig. 6(e)].[107] For the monochrome smartphone camera used in the study, a sensitivity down to 10 fluorophores could be determined. Recently, detection of single emitters on a SBFM could even be achieved by placing single fluorophores in the plasmonic hotspot of a DNA origami based nanoantenna.[94]

The high control over designed geometries and the breadboard character of DNA origami structures enables the creation of reference structures also for other imaging methods besides optical fluorescence microscopy. For example, placing plasmonic nanoparticles on a 24 helix-bundle DNA origami as shown in Fig. 7(a) forms chiral nanorulers especially suitable for 3D tomography or electron microscopy (EM).[112,113] The nanorulers of pure chirality (either left-handed L or right-handed R conformation) can easily be detected with EM due to their high contrast and show circular dichroism (CD) due to plasmonic resonance of the chirally labeled nanoparticles. In electron tomography, such chiral nanorulers were used as reference structures to determine the left-handed chirality of macrofibrils in mammalian hair.[114,115]

Besides placing modifications on DNA origami for nanometrology, the designed structural geometry of the DNA origami itself can

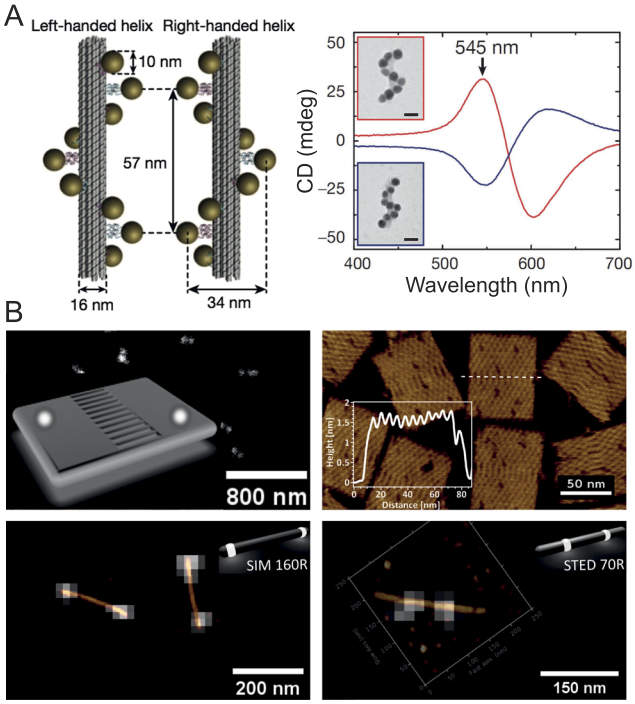

FIG. 7. (a) Left: Left- and right-handed nanohelices with nine gold nanoparticles attached to 24-helixbundle DNA origami. Right: Exemplary corresponding CD spectra of L (red) and R (blue) nanohelices. Insets show TEM images of corresponding nanohelices (scale bars, 20 nm).[112] (b) Top left: Sketch of a DNA rectangular origami (GATTA-AFM) with the theoretical locations for the Atto647N fluorophores. Background shows an STED image of the corresponding nanorulers. Top right: Fast amplitude modulation (AM) AFM image of the DNA origami lattice. The inset represents a cross-section across the central ladder seam of the DNA nanostructure (z-scale: 2 nm). Bottom: Optical correlation of consecutively acquired STED and AFM images of (left) SIM160R and (right) STED70R nanoruler (GATTAquant GmbH) with corresponding sketches.[116]

TABLE I. Overview of typical used DNA origami nanorulers for different fluorescence microscopy techniques.

Microscopy techniques	Distance/nm	Number of fluorophores per spot
MINFLUX 2D[10]/3D[11]	<10	1
STORM 2D[20,55,123]/3D[23]	30, 50, 90/180	6/10
DNA-PAINT 2D[19–21]/3D[63]	<10, 20, 40, 80/30, 80	1–6/10
SIM[122]	140	20
Confocal[20]	270–350	20
STED 2D[75]/3D[82]	50, 70, 90/80	20/15

be used as a nanoruler. By designing the stapling of the scaffold strand, structural characteristics of known geometry can be introduced into the DNA origami. This can be used to design topological nanorulers for scanning probe microscopy (SPM).[27] Figure 7(b) top images show an atomic force microscopy (AFM) nanoruler based on a rectangular DNA origami.[116] The depicted AFM nanoruler exhibits a central ladder seam bridging the crossed halves with a pitch of 6 nm, which can be used as a reference structure for quantitative AFM analysis [Fig. 7(b) top right]. Combining controlled positioning of fluorophores on the DNA origami and the design of the geometrical structure itself makes it a powerful tool for correlating AFM and optical microscopy. Exemplary optical correlation of STED and AFM for 160 nm and 70 nm nanorulers is shown in Fig. 7(b) bottom. The consecutively acquired STED and AFM images underline the accurately designed geometries of the fluorophore marks and the nanoruler itself. Additionally, combining the topographic information of AFM with the tip induced quenching of labeled fluorophores on DNA origami enabled correlative localization studies with sub 5 nm resolution.[117] DNA origami reference structures were also successfully used to investigate the production of singlet oxygen from a single photosensitizer molecule conjugated to the nanoruler. The subsequent diffusion of the singlet oxygen could be visualized by placing singlet oxygen cleavable linker molecules with biotin labels in designed distances to the photosensitizer molecule. After binding of streptavidin to the remaining linker molecules with biotin labels, the diffusion radii of the produced singlet oxygen molecules could be examined via AFM imaging.[118]

Also, the combination of confocal microscopy with an ABEL trap uses DNA origami nanorulers to test the performance of the setup.[119] The ABEL trap is an electrophoretic system, which tracks small particles via fluorescence and applies an electrokinetic feedback, which cancels the Brownian motion of the particle, thus trapping the particle.[120]

On one hand, the fluorophore of the DNA origami nanoruler is used to detect the DNA origami and control the anti-Brownian electrokinetic trap (ABEL trap). On the other hand, the origami aspect was used to explore different hydrodynamic radii, hence diffusion coefficients, and test the performance of this setup.

VI. CONCLUSION

DNA origami nanorulers provide an unprecedented control of shape and stoichiometry of impressively large objects. The simplicity of fabrication and the chemical robustness have enabled DNA origami to become the scaffold for reference structures in several fields of research and technology. In this perspective, we highlight the emerging applications in optical microscopy, scanning probe microscopy, and electron microscopy. In the meantime, even manufacturers of microscopes promote their products using DNA origami nanoruler demonstration.[121,122] On the other hand, DNA origami nanorulers as a ubiquitously available single-molecule standard can help customers to decide which microscope to purchase for a specific application and are frequently used as positive control for training the respective microscopy technique.

Typical and commonly used DNA origami nanorulers for different fluorescence microscopy techniques are listed in Table I with the required distances and fluorophore numbers.

For the future, we expect an ever-growing applicability of DNA origami nanorulers, brightness references, and further emerging applications in the fields of cytometry, microfluidics, and molecular diagnostics as well as fluorescence and correlative microscopy. As new functionalities are easily added for targeting the DNA origami to different local environments and binding partners, DNA reference structures have the potential to report on local events and to work *in situ* in complex chemical environments.

AUTHORS' CONTRIBUTIONS

M.S., J.B., and J.Z. contributed equally to this work.

ACKNOWLEDGMENTS

The authors thank Carsten Forthmann and Jürgen Schmied for their input and discussions. We gratefully acknowledge financial support from the DFG (Grant No. INST 86/1904-1 FUGG, TI 329/9-2, excellence clusters NIM and e-conversion, SFB1032), BMBF (Grant Nos. POCEMON, 13N14336, and SIBOF, 03VP03891), and the European Union's Horizon 2020 research and innovation program under Grant Agreement No. 737089 (Chipscope).

DATA AVAILABILITY

Data sharing is not applicable to this article as no new data were created or analyzed in this study.

REFERENCES

[1]S. W. Hell, S. J. Sahl, M. Bates, X. Zhuang, R. Heintzmann, M. J. Booth, J. Bewersdorf, G. Shtengel, H. Hess, P. Tinnefeld, A. Honigmann, S. Jakobs, I. Testa, L. Cognet, B. Lounis, H. Ewers, S. J. Davis, C. Eggeling, D. Klenerman, K. I. Willig, G. Vicidomini, M. Castello, A. Diaspro, and T. Cordes, J. Phys. D: Appl. Phys. **48**, 443001 (2015).
[2]D. Baddeley and J. Bewersdorf, Annu. Rev. Biochem. **87**, 965 (2018).
[3]G. Jacquemet, A. F. Carisey, H. Hamidi, R. Henriques, and C. Leterrier, J. Cell Sci. **133**, jcs240713 (2020).
[4]T. A. Klar, S. Jakobs, M. Dyba, A. Egner, and S. W. Hell, Proc. Natl. Acad. Sci. U. S. A. **97**, 8206 (2000).
[5]M. J. Rust, M. Bates, and X. Zhuang, Nat. Methods **3**, 793 (2006).
[6]M. Heilemann, S. van de Linde, M. Schüttpelz, R. Kasper, B. Seefeldt, A. Mukherjee, P. Tinnefeld, and M. Sauer, Angew. Chem. **120**, 6266 (2008).
[7]E. Betzig, G. H. Patterson, R. Sougrat, O. W. Lindwasser, S. Olenych, J. S. Bonifacino, M. W. Davidson, J. Lippincott-Schwartz, and H. F. Hess, Science **313**, 1642 (2006).

[8]A. Sharonov and R. M. Hochstrasser, Proc. Natl. Acad. Sci. U. S. A. **103**, 18911 (2006).
[9]R. Jungmann, C. Steinhauer, M. Scheible, A. Kuzyk, P. Tinnefeld, and F. C. Simmel, Nano Lett. **10**, 4756 (2010).
[10]F. Balzarotti, Y. Eilers, K. C. Gwosch, A. H. Gynnå, V. Westphal, F. D. Stefani, J. Elf, and S. W. Hell, Science **355**, 606 (2017).
[11]K. C. Gwosch, J. K. Pape, F. Balzarotti, P. Hoess, J. Ellenberg, J. Ries, and S. W. Hell, Nat. Methods **17**, 217 (2020).
[12]M. G. L. Gustafsson, Proc. Natl. Acad. Sci. U. S. A. **102**, 13081 (2005).
[13]M. G. L. Gustafsson, J. Microsc. **198**, 82 (2000).
[14]C. Steinhauer, R. Jungmann, T. L. Sobey, F. C. Simmel, and P. Tinnefeld, Angew. Chem., Int. Ed. **48**, 8870 (2009).
[15]A. Descloux, K. S. Grußmayer, and A. Radenovic, Nat. Methods **16**, 918 (2019).
[16]N. Banterle, K. H. Bui, E. A. Lemke, and M. Beck, J. Struct. Biol. **183**, 363 (2013).
[17]J. V. Thevathasan, M. Kahnwald, K. Cieśliński, P. Hoess, S. K. Peneti, M. Reitberger, D. Heid, K. C. Kasuba, S. J. Hoerner, Y. Li, Y.-L. Wu, M. Mund, U. Matti, P. M. Pereira, R. Henriques, B. Nijmeijer, M. Kueblbeck, V. J. Sabinina, J. Ellenberg, and J. Ries, Nat. Methods **16**, 1045 (2019).
[18]U. Endesfelder and M. Heilemann, Nat. Methods **11**, 235 (2014).
[19]J. J. Schmied, M. Raab, C. Forthmann, E. Pibiri, B. Wünsch, T. Dammeyer, and P. Tinnefeld, Nat. Protoc. **9**, 1367 (2014).
[20]J. J. Schmied, A. Gietl, P. Holzmeister, C. Forthmann, C. Steinhauer, T. Dammeyer, and P. Tinnefeld, Nat. Methods **9**, 1133 (2012).
[21]M. Raab, J. J. Schmied, I. Jusuk, C. Forthmann, and P. Tinnefeld, ChemPhysChem **15**, 2431 (2014).
[22]C. Steinhauer, R. Jungmann, T. L. Sobey, F. C. Simmel, and P. Tinnefeld, Angew. Chem. **121**, 9030 (2009).
[23]J. J. Schmied, C. Forthmann, E. Pibiri, B. Lalkens, P. Nickels, T. Liedl, and P. Tinnefeld, Nano Lett. **13**, 781 (2013).
[24]P. W. K. Rothemund, Nature **440**, 297 (2006).
[25]S. M. Douglas, H. Dietz, T. Liedl, B. Högberg, F. Graf, and W. M. Shih, Nature **459**, 414 (2009).
[26]C. E. Castro, F. Kilchherr, D.-N. Kim, E. L. Shiao, T. Wauer, P. Wortmann, M. Bathe, and H. Dietz, Nat. Methods **8**, 221 (2011).
[27]Y. Ke, S. Lindsay, Y. Chang, Y. Liu, and H. Yan, Science **319**, 180 (2008).
[28]M. Raab, I. Jusuk, J. Molle, E. Buhr, B. Bodermann, D. Bergmann, H. Bosse, and P. Tinnefeld, Sci. Rep. **8**, 1780 (2018).
[29]S. Beater, M. Raab, and P. Tinnefeld, *Methods in Cell Biology* (Academic Press, Inc., 2014), pp. 449–466.
[30]X.-C. Bai, T. G. Martin, S. H. W. Scheres, and H. Dietz, Proc. Natl. Acad. Sci. U. S. A. **109**, 20012 (2012).
[31]S. Fischer, C. Hartl, K. Frank, J. O. Rädler, T. Liedl, and B. Nickel, Nano Lett. **16**, 4282 (2016).
[32]J. J. Funke and H. Dietz, Nat. Nanotechnol. **11**, 47 (2016).
[33]M. T. Strauss, F. Schueder, D. Haas, P. C. Nickels, and R. Jungmann, Nat. Commun. **9**, 1600 (2018).
[34]A. Shaw, I. T. Hoffecker, I. Smyrlaki, J. Rosa, A. Grevys, D. Bratlie, I. Sandlie, T. E. Michaelsen, J. T. Andersen, and B. Högberg, Nat. Nanotechnol. **14**, 184 (2019).
[35]T. Schröder, M. B. Scheible, F. Steiner, J. Vogelsang, and P. Tinnefeld, Nano Lett. **19**, 1275 (2019).
[36]R. Iinuma, Y. Ke, R. Jungmann, T. Schlichthaerle, J. B. Woehrstein, and P. Yin, Science **344**, 65 (2014).
[37]S. J. Sahl, S. W. Hell, and S. Jakobs, Nat. Rev. Mol. Cell Biol. **18**, 685 (2017).
[38]M. Sauer and M. Heilemann, Chem. Rev. **117**, 7478 (2017).
[39]A. Jimenez, K. Friedl, and C. Leterrier, Methods **174**, 100 (2020).
[40]J. Fölling, M. Bossi, H. Bock, R. Medda, C. A. Wurm, B. Hein, S. Jakobs, C. Eggeling, and S. W. Hell, Nat. Methods **5**, 943 (2008).
[41]T. Dertinger, R. Colyer, G. Iyer, S. Weiss, and J. Enderlein, Proc. Natl. Acad. Sci. U. S. A. **106**, 22287 (2009).
[42]G. Giannone, E. Hosy, F. Levet, A. Constals, K. Schulze, A. I. Sobolevsky, M. P. Rosconi, E. Gouaux, R. Tampé, D. Choquet, and L. Cognet, Biophys. J. **99**, 1303 (2010).
[43]G. Patterson, M. Davidson, S. Manley, and J. Lippincott-Schwartz, Annu. Rev. Phys. Chem. **61**, 345 (2010).
[44]S. Tajada, C. M. Moreno, O. Samantha, S. Woods, D. Sato, M. F. Navedo, and L. F. Santana, J. Gen. Physiol. **149**, 639 (2017).
[45]Y. G. Suárez, J. L. Martínez, D. T. Hernández, H. O. Hernández, A. Pérez-Delgado, M. Méndez, C. D. Wood, J. M. Rendon-Mancha, D. Silva-Ayala, S. López, A. Guerrero, and C. F. Arias, Elife **8**, e42906 (2019).
[46]H. A. T. Pritchard, P. W. Pires, E. Yamasaki, P. Thakore, and S. Earley, Proc. Natl. Acad. Sci. U. S. A. **115**, E9745 (2018).
[47]H. A. T. Pritchard, C. S. Griffin, E. Yamasaki, P. Thakore, C. Lane, A. S. Greenstein, and S. Earley, Proc. Natl. Acad. Sci. U. S. A. **116**, 21874 (2019).
[48]K. J. A. Martens, S. P. B. van Beljouw, S. van der Els, J. N. A. Vink, S. Baas, G. A. Vogelaar, S. J. J. Brouns, P. van Baarlen, M. Kleerebezem, and J. Hohlbein, Nat. Commun. **10**, 3552 (2019).
[49]I. Jayasinghe, A. H. Clowsley, and C. Soeller, *Advances in Biomembranes and Lipid Self-Assembly*, edited by A. Iglič, M. Rappolt, and L. S.-A. García-Sáez (Academic Press, 2018), pp. 167–197.
[50]J. L. Davis, B. Dong, C. Sun, and H. F. Zhang, J. Biomed. Opt. **23**, 1 (2018).
[51]S. Mailfert, J. Touvier, L. Benyoussef, R. Fabre, A. Rabaoui, M.-C. Blache, Y. Hamon, S. Brustlein, S. Monneret, D. Marguet, and N. Bertaux, Biophys. J. **115**, 565 (2018).
[52]R. J. Marsh, K. Pfisterer, P. Bennett, L. M. Hirvonen, M. Gautel, G. E. Jones, and S. Cox, Nat. Methods **15**, 689 (2018).
[53]A. D. Staszowska, P. Fox-Roberts, L. M. Hirvonen, C. J. Peddie, L. M. Collinson, G. E. Jones, and S. Cox, Bioinformatics **34**, 4102 (2018).
[54]M. Fazel, M. J. Wester, B. Rieger, R. Jungmann, and K. A. Lidke, bioRxiv 752287 (2019).
[55]R. Diekmann, Ø. I. Helle, C. I. Øie, P. McCourt, T. R. Huser, M. Schüttpelz, and B. S. Ahluwalia, Nat. Photonics **11**, 322 (2017).
[56]I. Gyongy, A. Davies, N. A. W. Dutton, R. R. Duncan, C. Rickman, R. K. Henderson, and P. A. Dalgarno, Sci. Rep. **6**, 37349 (2016).
[57]I. M. Antolovic, S. Burri, C. Bruschini, R. A. Hoebe, and E. Charbon, Sci. Rep. **7**, 44108 (2017).
[58]M. Caccia, L. Nardo, R. Santoro, and D. Schaffhauser, Nucl. Instrum. Methods Phys. Res., Sect. A **926**, 101 (2019).
[59]S. Coelho, J. Baek, M. S. Graus, J. M. Halstead, P. R. Nicovich, K. Feher, H. Gandhi, J. J. Gooding, and K. Gaus, Sci. Adv. **6**, eaay8271 (2020).
[60]J. Schnitzbauer, M. T. Strauss, T. Schlichthaerle, F. Schueder, and R. Jungmann, Nat. Protoc. **12**, 1198 (2017).
[61]M. Ovesný, P. Křížek, J. Borkovec, Z. Švindrych, and G. M. Hagen, Bioinformatics **30**, 2389 (2014).
[62]J. Schmied, Opt. Photonik **11**, 23 (2016).
[63]R. Lin, A. H. Clowsley, T. Lutz, D. Baddeley, and C. Soeller, Methods **174**, 56 (2020).
[64]R. Jungmann, M. S. Avendaño, M. Dai, J. B. Woehrstein, S. S. Agasti, Z. Feiger, A. Rodal, and P. Yin, Nat. Methods **13**, 439 (2016).
[65]O. K. Wade, J. B. Woehrstein, P. C. Nickels, S. Strauss, F. Stehr, J. Stein, F. Schueder, M. T. Strauss, M. Ganji, J. Schnitzbauer, H. Grabmayr, P. Yin, P. Schwille, and R. Jungmann, Nano Lett. **19**, 2641 (2019).
[66]F. Schueder, J. Stein, F. Stehr, A. Auer, B. Sperl, M. T. Strauss, P. Schwille, and R. Jungmann, Nat. Methods **16**, 1101 (2019).
[67]S. Strauss and R. Jungmann, Nat. Methods **17**, 789 (2020).
[68]M. F. Juette, T. J. Gould, M. D. Lessard, M. J. Mlodzianoski, B. S. Nagpure, B. T. Bennett, S. T. Hess, and J. Bewersdorf, Nat. Methods **5**, 527 (2008).
[69]B. Huang, W. Wang, M. Bates, and X. Zhuang, Science **319**, 810 (2008).
[70]M. Raab, C. Vietz, F. D. Stefani, G. P. Acuna, and P. Tinnefeld, Nat. Commun. **8**, 13966 (2017).
[71]L. E. Weiss, Y. S. Ezra, S. Goldberg, B. Ferdman, O. Adir, A. Schroeder, O. Alalouf, and Y. Shechtman, Nat. Nanotechnol. **15**, 500 (2020).
[72]K. K. H. Chung, Z. Zhang, P. Kidd, Y. Zhang, N. D. Williams, B. Rollins, Y. Yang, C. Lin, D. Baddeley, and J. Bewersdorf, bioRxiv:066886 (2020).
[73]S. W. Hell and J. Wichmann, Opt. Lett. **19**, 780 (1994).

[74]C. A. Combs, D. L. Sackett, and J. R. Knutson, J. Microsc. **274**, 168 (2019).
[75]S. C. Sidenstein, E. D'Este, M. J. Böhm, J. G. Danzl, V. N. Belov, and S. W. Hell, Sci. Rep. **6**, 26725 (2016).
[76]S. Schedin-Weiss, I. Caesar, B. Winblad, H. Blom, and L. O. Tjernberg, Acta Neuropathol. Commun. **4**, 29 (2016).
[77]T. J. Nicholls, C. A. Nadalutti, E. Motori, E. W. Sommerville, G. S. Gorman, S. Basu, E. Hoberg, D. M. Turnbull, P. F. Chinnery, N.-G. Larsson, E. Larsson, M. Falkenberg, R. W. Taylor, J. D. Griffith, and C. M. Gustafsson, Mol. Cell **69**, 9 (2018).
[78]J. J. S. J. J. Schmied, R. Dijkstra, M. Scheible, and G. M. R. De Luca, "Measuring the 3D STED-PSF with a new type of fluorescent beads," available at https://www.leica-microsystems.com/science-lab/measuring-the-3d-sted-psf-with-a-new-type-of-fluorescent-beads/.
[79]S. Beater, P. Holzmeister, E. Pibiri, B. Lalkens, and P. Tinnefeld, Phys. Chem. Chem. Phys. **16**, 6990 (2014).
[80]S. Beater, P. Holzmeister, B. Lalkens, and P. Tinnefeld, Opt. Express **23**, 8630 (2015).
[81]R. Jungmann, M. S. Avendaño, J. B. Woehrstein, M. Dai, W. M. Shih, and P. Yin, Nat. Methods **11**, 313 (2014).
[82]F. Göttfert, T. Pleiner, J. Heine, V. Westphal, D. Görlich, S. J. Sahl, and S. W. Hell, Proc. Natl. Acad. Sci. U. S. A. **114**, 2125 (2017).
[83]J. Alvelid and I. Testa, J. Phys. D: Appl. Phys. **53**, ab4c13 (2020).
[84]A. Girsault and A. Meller, Opt. Lett. **45**, 2712 (2020).
[85]H. Ta, J. Keller, M. Haltmeier, S. K. Saka, J. Schmied, F. Opazo, P. Tinnefeld, A. Munk, and S. W. Hell, Nat. Commun. **6**, 7977 (2015).
[86]M. Oneto, L. Scipioni, M. J. Sarmento, I. Cainero, S. Pelicci, L. Furia, P. G. Pelicci, G. I. Dellino, P. Bianchini, M. Faretta, E. Gratton, A. Diaspro, and L. Lanzanò, Biophys. J. **117**, 2054 (2019).
[87]J. Cnossen, T. Hinsdale, R. Thorsen, M. Siemons, F. Schueder, R. Jungmann, C. S. Smith, B. Rieger, and S. Stallinga, Nat. Methods **17**, 59 (2020).
[88]L. Gu, Y. Li, S. Zhang, Y. Xue, W. Li, D. Li, T. Xu, and W. Ji, Nat. Methods **16**, 1114 (2019).
[89]L. Stryer and R. P. Haugland, Proc. Natl. Acad. Sci. U. S. A. **58**, 719 (1967).
[90]I. H. Stein, V. Schüller, P. Böhm, P. Tinnefeld, and T. Liedl, ChemPhysChem **12**, 689 (2011).
[91]E. S. Andersen, M. Dong, M. M. Nielsen, K. Jahn, R. Subramani, W. Mamdouh, M. M. Golas, B. Sander, H. Stark, C. L. P. Oliveira, J. S. Pedersen, V. Birkedal, F. Besenbacher, K. V. Gothelf, and J. Kjems, Nature **459**, 73 (2009).
[92]G. P. Acuna, M. Bucher, I. H. Stein, C. Steinhauer, A. Kuzyk, P. Holzmeister, R. Schreiber, A. Moroz, F. D. Stefani, T. Liedl, F. C. Simmel, and P. Tinnefeld, ACS Nano **6**, 3189 (2012).
[93]G. P. Acuna, F. M. Möller, P. Holzmeister, S. Beater, B. Lalkens, and P. Tinnefeld, Science **338**, 506 (2012).
[94]K. Trofymchuk, V. Glembockyte, L. Grabenhorst, F. Steiner, C. Vietz, C. Close, M. Pfeiffer, L. Richter, M. L. Schütte, F. Selbach, R. Yaadav, J. Zähringer, Q. Wei, A. Ozcan, B. Lalkens, G. P. Acuna, and P. Tinnefeld, bioRxiv:2020.04.09.032037 (2020).
[95]N. Aissaoui, K. Moth-Poulsen, M. Käll, P. Johansson, L. M. Wilhelmsson, and B. Albinsson, Nanoscale **9**, 673 (2017).
[96]J. Bohlen, Á. Cuartero-González, E. Pibiri, D. Ruhlandt, A. I. Fernández-Domínguez, P. Tinnefeld, and G. P. Acuna, Nanoscale **11**, 7674 (2019).
[97]K. Korobchevskaya, B. Lagerholm, H. Colin-York, and M. Fritzsche, Photonics **4**, 41 (2017).
[98]S. Isbaner, N. Karedla, I. Kaminska, D. Ruhlandt, M. Raab, J. Bohlen, A. Chizhik, I. Gregor, P. Tinnefeld, J. Enderlein, and R. Tsukanov, Nano Lett. **18**, 2616 (2018).
[99]I. Kaminska, J. Bohlen, S. Rocchetti, F. Selbach, G. P. Acuna, and P. Tinnefeld, Nano Lett. **19**, 4257 (2019).
[100]A. Ghosh, A. Sharma, A. I. Chizhik, S. Isbaner, D. Ruhlandt, R. Tsukanov, I. Gregor, N. Karedla, and J. Enderlein, Nat. Photonics **13**, 860 (2019).
[101]F. Chen, P. W. Tillberg, and E. S. Boyden, Science **347**, 543 (2015).
[102]J.-B. Chang, F. Chen, Y.-G. Yoon, E. E. Jung, H. Babcock, J. S. Kang, S. Asano, H.-J. Suk, N. Pak, P. W. Tillberg, A. T. Wassie, D. Cai, and E. S. Boyden, Nat. Methods **14**, 593 (2017).
[103]Y. Wang, Z. Yu, C. K. Cahoon, T. Parmely, N. Thomas, J. R. Unruh, B. D. Slaughter, and R. S. Hawley, Nat. Protoc. **13**, 1869 (2018).
[104]A. R. Halpern, G. C. M. Alas, T. J. Chozinski, A. R. Paredez, and J. C. Vaughan, ACS Nano **11**, 12677 (2017).
[105]M. B. Scheible and P. Tinnefeld, bioRxiv:265405 (2018).
[106]V. C. Coffman and J.-Q. Wu, Mol. Biol. Cell **25**, 1545 (2014).
[107]C. Vietz, M. L. Schütte, Q. Wei, L. Richter, B. Lalkens, A. Ozcan, P. Tinnefeld, and G. P. Acuna, ACS Omega **4**, 637 (2019).
[108]A. Schwartz, A. K. Gaigalas, L. Wang, G. E. Marti, R. F. Vogt, and E. Fernandez-Repollet, Cytometry, Part B **57B**, 1 (2004).
[109]L. D. Smith, Y. Liu, M. U. Zahid, T. D. Canady, L. Wang, M. Kohli, B. T. Cunningham, and A. M. Smith, ACS Nano **14**, 2324 (2020).
[110]A. Kurz, J. J. Schmied, K. S. Grußmayer, P. Holzmeister, P. Tinnefeld, and D.-P. Herten, Small **9**, 4061 (2013).
[111]Q. Wei, G. Acuna, S. Kim, C. Vietz, D. Tseng, J. Chae, D. Shir, W. Luo, P. Tinnefeld, and A. Ozcan, Sci. Rep. **7**, 2124 (2017).
[112]A. Kuzyk, R. Schreiber, Z. Fan, G. Pardatscher, E.-M. Roller, A. Högele, F. C. Simmel, A. O. Govorov, and T. Liedl, Nature **483**, 311 (2012).
[113]A. Briegel, M. Pilhofer, D. N. Mastronarde, and G. J. Jensen, J. Struct. Biol. **183**, 95 (2013).
[114]D. P. Harland, V. Novotna, M. Richena, S. Velamoor, M. Bostina, and A. J. McKinnon, J. Struct. Biol. **206**, 345 (2019).
[115]D. P. Harland, V. Novotná, M. Richena, M. Bostina, S. Velamoor, and A. J. McKinnon, Microsc. Microanal. **25**, 1348 (2019).
[116]T. Neumann, J. Barner, and D. Stamov, JPK Application Note 1, 2014.
[117]O. Schulz, Z. Zhao, A. Ward, M. Koenig, F. Koberling, Y. Liu, J. Enderlein, H. Yan, and R. Ros, Opt. Nanosc. **2**, 1 (2013).
[118]S. Helmig, A. Rotaru, D. Arian, L. Kovbasyuk, J. Arnbjerg, P. R. Ogilby, J. Kjems, A. Mokhir, F. Besenbacher, and K. V. Gothelf, ACS Nano **4**, 7475 (2010).
[119]M. Dienerowitz, F. Dienerowitz, and M. Börsch, J. Opt. **20**, 034006 (2018).
[120]A. E. Cohen and W. E. Moerner, Appl. Phys. Lett. **86**, 093109 (2005).
[121]J. Huff, W. Bathe, R. Netz, T. Anhut, and K. Weisshart, Technology Note by ZEISS 1, 2015.
[122]R. T. Borlinghaus and C. Kappel, Nat. Methods **13**, i (2016).
[123]L. Wang, B. Bateman, L. C. Zanetti-Domingues, A. N. Moores, S. Astbury, C. Spindloe, M. C. Darrow, M. Romano, S. R. Needham, K. Beis, D. J. Rolfe, D. T. Clarke, and M. L. Martin-Fernandez, Commun. Biol. **2**, 74 (2019).